

CHANDRA LOW ENERGY TRANSMISSION GRATING SPECTRUM OF SS CYGNI IN OUTBURST

CHRISTOPHER W. MAUCHE¹

Lawrence Livermore National Laboratory, L-473, 7000 East Avenue, Livermore, CA 94550
 mauche@cygnus.llnl.gov

Accepted for publication in *Astrophysical Journal* 2004 March 30

ABSTRACT

We have fitted the *Chandra* Low Energy Transmission Grating spectrum of SS Cygni in outburst with a single temperature blackbody suffering the photoelectric opacity of a neutral column density and the scattering opacity of an outflowing wind. We find that this simple model is capable of reproducing the essential features of the observed spectrum with the blackbody temperature $T_{\text{bl}} \approx 250 \pm 50$ kK, hydrogen column density $N_{\text{H}} \approx 5.0^{+2.9}_{-1.5} \times 10^{19} \text{ cm}^{-2}$, fractional emitting area $f \approx 5.6^{+60}_{-4.5} \times 10^{-3}$, boundary layer luminosity $L_{\text{bl}} \approx 5^{+18}_{-3} \times 10^{33} \text{ erg s}^{-1}$, wind velocity $v \approx 2500 \text{ km s}^{-1}$, wind mass-loss rate $\dot{M}_{\text{w}} \approx 1.1 \times 10^{16} \text{ g s}^{-1}$, and arbitrary values of the wind ionization fractions of 20 ions of O, Ne, Mg, Si, S, and Fe. Given that in outburst the accretion disk luminosity $L_{\text{disk}} \approx 1 \times 10^{35} \text{ erg s}^{-1}$, $L_{\text{bl}}/L_{\text{disk}} \approx 0.05^{+0.18}_{-0.03}$, which can be explained if the white dwarf (or an equatorial belt thereon) is rotating with an angular velocity $\Omega_{\text{wd}} \approx 0.7^{+0.1}_{-0.2} \text{ Hz}$, hence $V_{\text{rot}} \sin i \sim 2300 \text{ km s}^{-1}$.

Subject headings: accretion, accretion disks — binaries: close — novae, cataclysmic variables — stars: individual (SS Cygni) — X-rays: binaries

1. INTRODUCTION

According to simple theory, the boundary layer between the accretion disk and the surface of the white dwarf is the dominant source of high energy radiation in nonmagnetic cataclysmic variables (CVs). Unless the white dwarf is rotating rapidly, the boundary layer luminosity $L_{\text{bl}} \approx GM_{\text{wd}}\dot{M}/2R_{\text{wd}}$, where M_{wd} and R_{wd} are respectively the mass and radius of the white dwarf and \dot{M} is the mass-accretion rate. When \dot{M} is low, as in dwarf nova in quiescence, the boundary layer is optically thin to its own radiation and its temperature is of order the virial temperature $T_{\text{vir}} = GM_{\text{wd}}m_{\text{H}}/3kR_{\text{wd}} \sim 10 \text{ keV}$. When \dot{M} is high, as in nova-like variables and dwarf novae in outburst, the boundary layer is optically thick to its own radiation and its temperature is of order the blackbody temperature $T_{\text{bb}} = (GM_{\text{wd}}\dot{M}/8\pi\sigma f R_{\text{wd}}^3)^{1/4} \sim 100 \text{ kK}$.

The compact nature of the boundary layer is established by the narrow eclipses of the hard X-ray flux of high inclination dwarf novae in quiescence (Wood et al. 1995; Mukai et al. 1997; van Teeseling 1997; Pratt et al. 1999a; Wheatley & West 2003) and the short periods [$P \sim 10 \text{ s} \sim 2\pi(R_{\text{wd}}^3/GM_{\text{wd}})^{1/2}$] of the oscillations of the soft X-ray and extreme ultraviolet (EUV) flux of nova-like variables and dwarf novae in outburst (Warner 2004; Mauche 2004). However, an *extended* source of soft X-ray and EUV flux is required to explain the lack of eclipses in high inclination nova-like variables and dwarf novae in outburst (Naylor et al. 1988; Wood, Naylor, & Marsh 1995; Pratt et al. 1999b; Mauche & Raymond 2000; Pratt et al. 2004).

Using the *Extreme Ultraviolet Explorer* (EUVE) light curve and spectrum of OY Car in superoutburst, Mauche & Raymond (2000) argued that the source of the extended EUV flux of high- \dot{M} nonmagnetic CVs is the accretion disk wind. In this picture, in high inclination systems the boundary layer is hidden by the accretion disk for all binary phases, but its flux is scattered into the line of sight by resonance transitions of ions in the wind. Because the scattering optical depths of these transitions are much higher than the Thompson optical depth, the EUV spec-

tra of such systems should be dominated by broad lines.

Consistent with this picture, in outburst the EUV spectra of the high inclination dwarf novae OY Car ($i \approx 83^\circ$; Mauche & Raymond 2000) and WZ Sge ($i \approx 75^\circ$; Wheatley & Mauche 2004, in preparation) are dominated by broad lines, while that of the low inclination dwarf novae VW Hyi ($i \sim 60^\circ$; Mauche 1996) and SS Cyg ($i \sim 40^\circ$; Mauche, Raymond, & Mattei 1995) are dominated by the continuum. U Gem ($i \approx 70^\circ$; Long et al. 1996) is a transitional case, as its EUV flux is partially eclipsed and its EUV spectrum contains of broad emission lines superposed on a bright continuum.

The general case of the radiation transfer of the boundary layer flux through the accretion disk wind is complicated, but schematically we expect that in high inclination systems the EUV spectrum will be of the form $F_{\lambda} e^{-\tau'_{\lambda}} (1 - e^{-\tau_{\lambda}})$, while in low inclination systems it will be of the form $F_{\lambda} e^{-\tau'_{\lambda}} e^{-\tau_{\lambda}}$, where F_{λ} is the intrinsic boundary layer spectrum, τ'_{λ} is the photoelectric optical depth of the wind and the interstellar medium, and τ_{λ} is the scattering optical depth of the wind. Mauche & Raymond (2000) showed that the second version of this model describes the main features of the EUVE spectrum of OY Car in superoutburst, and we show here that the first version of this model describes the main features of the *Chandra* Low Energy Transmission Grating (LETG) spectrum of SS Cyg in outburst. A preliminary discussion of this spectrum is supplied by Mauche (2004), while the quasi-coherent oscillations of the EUV flux is discussed by Mauche (2002).

2. CHANDRA OBSERVATION AND DATA ANALYSIS

Our pre-approved target-of-opportunity *Chandra* LETG plus High Resolution Camera (HRC) observation of SS Cyg was performed between 2001 January 16 21^h13^m and January 17 10^h50^m UT during the plateau phase of a wide normal (asymmetric) dwarf nova outburst that began on January 12 (Fig. 1). When the observation began, SS Cyg had been at maximum optical light ($V \approx 8.5$) for approximately $3\frac{1}{2}$ days; long enough,

¹ This paper is dedicated to the memory and accomplishments of my colleague and friend Janet Akyüz Mattei, who died on 2004 March 22 after a long battle with acute myelogenous leukemia. Her passing is a great loss to the astronomical community, both amateur and professional.

given the delay of approximately $1\frac{1}{2}$ days between the rise of the optical and EUV light curves of SS Cyg (Mauche, Mattei, & Bateson 2001), for the EUV flux to have reached maximum and for the system to have reached a quasi-steady state. Indeed, the zero- and \pm first-order LETG/HRC count rates were roughly constant throughout the 47.3 ks observation at 1.5 and 4.9 counts s^{-1} , respectively.

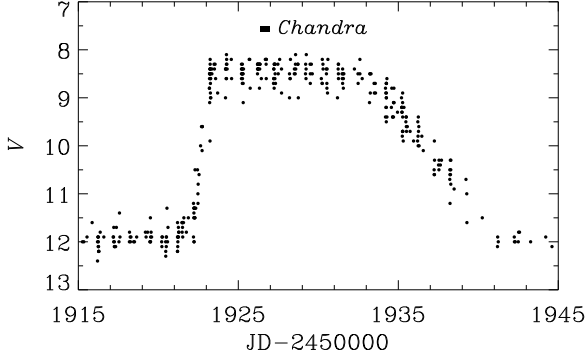


FIG. 1.— AAVSO light curve of SS Cyg (Mattei 2003). Black rectangle marks the interval of the *Chandra* LETG observation.

The files used for analysis were created on 2002 January 7 by the pipeline data reduction software using CIAO 2.0 with AS-DCS version 6.5.1. Events were extracted from the level 2 evt file, and the mean spectrum and source and background region masks were extracted from the level 2 pha file. The observation-average fluxed spectrum (units of $\text{erg cm}^{-2} \text{s}^{-1} \text{\AA}^{-1}$) was derived from the \pm first-order pha source and background count spectra and the “canned” \pm first-order LETG/HRC effective area files distributed with *Chandra* CALBD 2.21. To avoid the HRC chip gaps, the wave bands $\lambda = 60.2\text{--}67.2 \text{\AA}$ for the positive spectral order and $\lambda = 49.9\text{--}57.2 \text{\AA}$ for the negative spectral order were excluded. The spectrum used for subsequent analysis combines \pm first orders and is binned up in wavelength by a factor of four to $\Delta\lambda = 0.05 \text{\AA}$.

As shown by Mauche (2004), the resulting LETG spectrum contains two distinct components: (1) an X-ray component shortward of 42\AA consisting of a bremsstrahlung continuum and emission lines of H- and He-like C, N, O, Ne, Mg, and Si and L-shell Fe (most prominently Fe XVII) and (2) an EUV component extending from 42\AA to 130\AA that consists of a continuum significantly modified by a forest of broad absorption features (see Fig. 3). In the $72\text{--}130 \text{\AA}$ wave band, the LETG spectrum is essentially identical to that measured by the *EUVE* short wavelength spectrometer during the 1993 August (Mauche, Raymond, & Mattei 1995) and 1996 October (Wheatley, Mauche, & Mattei 2003) outbursts of SS Cyg. The X-ray component of the LETG spectrum is not discussed here further, but is understood to be due to the residual optically thin portion of the boundary layer.

3. SPECTRAL ANALYSIS

To fit the EUV spectrum of SS Cyg, we used the simple model described by Mauche & Raymond (2000), which assumes that the boundary layer spectrum is that of a single temperature blackbody suffering the photoelectric opacity of a neutral column density and the scattering opacity of an outflowing wind. The boundary layer spectrum is then specified by the blackbody temperature T_{bl} , fractional emitting area f (hence luminosity $L_{\text{bl}} = 4\pi f R_{\text{wd}}^2 \sigma T_{\text{bl}}^4$), and hydrogen column

density N_{H} (assuming the Rumph, Bowyer, & Vennes 1994 cross section with H I, He I, and He II with abundance ratios of 1:0.1:0.01). The properties of the wind are specified by its mass-loss rate $\dot{M}_0 = 4\pi r^2 \mu m_{\text{H}} n v = 7.0 \times 10^{15} \text{ g s}^{-1}$ via fiducial values of the wind radius $r = 10^{10} \text{ cm}$, density $n = 10^{10} \text{ cm}^{-3}$, and velocity $v = 2500 \text{ km s}^{-1}$, where the value of the wind velocity was chosen to reproduce the observed blueshift of the absorption lines. In the Sobolev approximation, the wind optical depth $\tau_{\lambda} = (\pi e^2 / m_e c) n A X \lambda_{ij} f_{ij} (g_i / \sum g_i) (dv/dr)^{-1}$, where $dv/dr = 2500 \text{ km s}^{-1} / 10^{10} \text{ cm} = 0.025 \text{ s}^{-1}$ is the wind velocity gradient, λ_{ij} , f_{ij} , and g_i are respectively the wavelengths, oscillator strengths, and statistical weights of the various resonance transitions (Verner, Verner, & Ferland 1996), A are the elemental abundances relative to hydrogen (Anders & Grevesse 1989), X are the ionization fractions, and the other symbols have their usual meanings. To account for the velocity of the wind along the line of sight, the transition wavelengths were blueshifted by $\Delta\lambda_{ij} = \lambda_{ij} v / c$. To match the observed widths of the absorption lines, the opacity for all lines was distributed as a Gaussian with FWHM = 1.0\AA . Finally, we assumed that the source distance $d = 160 \text{ pc}$ (Harrison et al. 2000) and the white dwarf mass $M_{\text{wd}} = 1.0 M_{\odot}$, hence the white dwarf radius $R_{\text{wd}} = 5.5 \times 10^8 \text{ cm}$.

With these assumptions, the free parameters of the model are the boundary layer temperature T_{bl} , fractional emitting area f , hydrogen column density N_{H} , wind mass-loss rate $\dot{M}_w = m \times \dot{M}_0$, and ionization fractions X . Operationally, the model was fit to the data between 45\AA and 125\AA using a grid search in the variables T_{bl} , N_{H} , and m , with $X = 1$ and f determined by the model normalization that minimizes χ^2 between the model and the data. The resulting best-fit model has χ^2 per degree of freedom (dof) = $5961/1596 = 3.74$ with $T_{\text{bl}} = 250 \text{ kK}$, $N_{\text{H}} = 5.0 \times 10^{19} \text{ cm}^{-2}$, $f = 5.0 \times 10^{-3}$, and $m = 1.6$ and contains 34 lines of O V–O VI, Ne V–Ne VIII, Mg V–Mg X, Si V–Si XI, S VII–S X, Fe VII–Fe X, and Fe XII–Fe XV (31 ions of six elements) that depress the continuum by at least 10%. Next, T_{bl} , N_{H} , and m were frozen and X was allowed to vary for each of these 31 ions. Table 1 shows the evolution of χ^2 as sequential steps were taken in this new parameter space. The resulting best-fit model has $\chi^2/\text{dof} = 3333/1565 = 2.13$ with $f = 5.6 \times 10^{-3}$ and 41 lines of O V–O VI, Ne V–Ne VIII, Mg V–Mg IX, Si VI–Si IX, S VII, Fe VII, Fe IX, Fe XIII, and Fe XV (20 ions of six elements) that depress the continuum by at least 10%. The resulting contours of χ^2 and f in the $[T_{\text{bl}}, N_{\text{H}}]$ parameter plane are shown in Figure 2 and the best-fit model is shown superposed on the data in Figure 3.

With $\chi^2/\text{dof} = 2.13$, the fit shown in Figure 3 is unacceptable in a statistical sense, but it clearly reproduces the essential features of the observed spectrum. Ignoring the unmodeled C V He α emission feature at 41\AA , the largest systematic residuals between the model and the data are in the neighborhood of 48, 65, 86, and 92\AA , where the data is above the model, but this discrepancy probably could be accommodated in a more detailed model by raising the continuum and increasing the wind optical depth. The goodness of the fit is due in large part to the arbitrary variations of the ionization fractions, which decrease χ^2/dof from $5961/1596 = 3.74$ to $3333/1565 = 2.13$ after 14 steps in χ^2 space. The reasons for the sequential improvements in the fit documented in Table 1 are often clear [e.g., increasing $X(\text{Mg VIII})$ increases the depth of the model absorption features at $\approx 69.0 \text{\AA}$ and $\approx 74.4 \text{\AA}$; increasing $X(\text{Si VII})$ increases the depth of the model absorption features at $\approx 67.6 \text{\AA}$ and

$\approx 69.0 \text{ \AA}$; zeroing out $X(\text{Si V})$ removes a strong model absorption feature at $\approx 96.4 \text{ \AA}$, but others are less so [e.g., increasing $X(\text{Fe VII})$ increases the depth of a number of absorption features longward of $\approx 102 \text{ \AA}$]. While the individual values of the ionization fractions in Table 1 are not unreasonable, as a set they make little sense physically.

TABLE 1
Model Ionization Fractions

Ion	X	χ^2
Mg VIII.....	4.0	5210
Si VII.....	3.2	4742
Fe VII	10.	4276
Si V	0.0	4089
Mg VII	1.6	3938
Fe XIII.....	4.0	3775
Mg V	2.5	3660
Mg VI	0.5	3567
Fe XII	0.0	3511
S IX	0.0	3464
Ne VIII	0.6	3418
Si X	0.0	3383
Mg VIII.....	3.2	3352
Si VI	1.3	3333

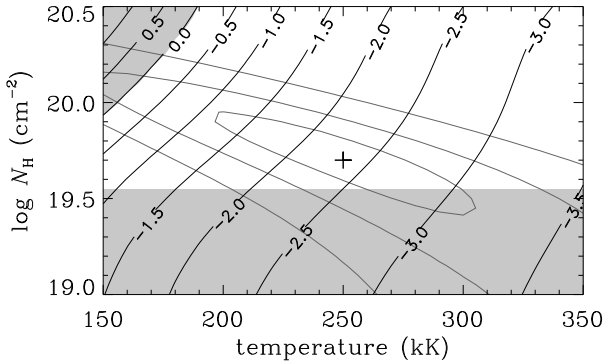


FIG. 2.— Contours of $\chi^2 = [1.5, 3, 6]\chi_{\min}^2$ (gray curves) and $\log f$ (black curves) in the $[T_{\text{bl}}, N_{\text{H}}]$ parameter plane for the model described in §3. Regions of parameter space shaded gray are excluded by the requirements that $N_{\text{H}} \geq 3.5 \times 10^{19} \text{ cm}^{-2}$ and $f \leq 1$. Cross marks the parameters of the model shown in Fig. 3.

To see this, we used XSTAR v1.07 to calculate the ionization fractions of a photoionized plasma for various values of the ionization parameter $\xi = L_{\text{bl}}/nr^2$. With $L_{\text{bl}} = 4\pi f R_{\text{wd}}^2 \sigma T_{\text{bl}}^4 = 4.7 \times 10^{33} \text{ erg s}^{-1}$ and the fiducial values of n and r , $\log \xi = 3.7$. Assuming that the plasma is optically thin and that the photoionizing source is a 250 kK blackbody, the XSTAR runs demonstrate that the ionization parameter must span the range $-1 \lesssim \log \xi \lesssim 5$ to account for the range of ions present in the model.

Given this result, we investigated whether it is possible to obtain good fits to the data with less arbitrary sets of ionization fractions. In the first attempt, we fixed the model parameters T_{bl} and N_{H} at their nominal values, set the ionization fractions equal to their peak values for $-1 \leq \log \xi \leq 5$, and adjusted m and f . This model produced only a small improvement in the fit relative to that with $X = 1$, since the peak ionization fractions differ by factors of only a few. In the second attempt, we weighted the ionization fraction distributions $X(\xi)$ by the function $e^{-\xi_{\min}/\xi} e^{-\xi/\xi_{\max}}$, which suppresses the ionization fractions

at the lower and upper ends of the range. However, varying the exponential cutoffs ξ_{\min} and ξ_{\max} and m and f again produced only a small improvement in the fit relative to that with $X = 1$. We conclude that our simple model is capable of producing reasonably good fits to the data only if the ionization fractions are allowed to vary arbitrarily.

4. DISCUSSION

We have fitted the *Chandra* LETG spectrum of SS Cyg in outburst with a single temperature blackbody suffering the photoelectric opacity of a neutral column density and the scattering opacity of an outflowing wind. The best-fit model, shown in Figure 3, has parameters $T_{\text{bl}} = 250 \text{ kK}$, $N_{\text{H}} = 5.0 \times 10^{19} \text{ cm}^{-2}$, $f = 5.6 \times 10^{-3}$, $\dot{M}_{\text{w}} = 1.1 \times 10^{16} \text{ g s}^{-1}$, and the values of X listed in Table 1 ($X = 1$ otherwise). Assuming that the wind is optically thin and photoionized by a 250 kK blackbody, the range of ions present in the model requires that the ionization parameter $-1 \lesssim \log \xi \lesssim 5$.

Given these results, in outburst the boundary layer luminosity $L_{\text{bl}} = 4.7 \times 10^{33} \text{ erg s}^{-1}$. A lower limit on the value of this quantity is imposed by the value of the interstellar H column density, which Mauche, Raymond, & Córdova (1988) estimated to be $3.5 \times 10^{19} \text{ cm}^{-2}$ based on the curve-of-growth of interstellar absorption lines in high resolution *International Ultraviolet Explorer* spectra of SS Cyg in outburst. For $-1 \lesssim \log \xi \lesssim 5$, H and He are fully ionized, so the wind should have no photoelectric opacity in the EUV bandpass, and N_{H} should be equal to the interstellar H column density. With $N_{\text{H}} = 3.5 \times 10^{19} \text{ cm}^{-2}$ and $T_{\text{bl}} = 300 \text{ kK}$, Figure 2 shows that $f = 1.1 \times 10^{-3}$, hence $L_{\text{bl}} = 1.7 \times 10^{33} \text{ erg s}^{-1}$. At the other end of the χ^2 ellipse, with $T_{\text{bl}} = 200 \text{ kK}$ and $N_{\text{H}} = 7.9 \times 10^{19} \text{ cm}^{-2}$, $f = 6.6 \times 10^{-2}$, hence $L_{\text{bl}} = 2.3 \times 10^{34} \text{ erg s}^{-1}$. We conclude that a reasonable estimate of the boundary layer luminosity $L_{\text{bl}} \approx 5_{-3}^{+18} \times 10^{33} (d/160 \text{ pc})^2 \text{ erg s}^{-1}$.

How does this compare with the accretion disk luminosity? Polidan & Holberg (1984) used optical through far ultraviolet spectra of SS Cyg in outburst to determine that $L_{\text{disk}} \approx 1 \times 10^{35} (d/160 \text{ pc})^2 \text{ erg s}^{-1}$, so $L_{\text{bl}}/L_{\text{disk}} \approx 0.05_{-0.03}^{+0.18}$. Theoretically, we expect that this ratio is equal to one unless the white dwarf is rotating rapidly, in which case $L_{\text{bl}}/L_{\text{disk}} = (1 - \omega)^2$, where $\omega = \Omega_{\text{wd}}/\Omega_{\text{K}}(R_{\text{wd}})$, $\Omega_{\text{wd}} = 2\pi/P_{\text{spin}}$ is the angular velocity of the white dwarf, and $\Omega_{\text{K}}(R_{\text{wd}}) = (GM_{\text{wd}}/R_{\text{wd}}^3)^{1/2} \approx 0.9 \text{ Hz}$ is the Keplerian angular velocity of material just above its surface (Popham & Narayan 1995). The white dwarf can be spun up to the required rate by accreting an amount of mass $\Delta M = M_{\text{wd}} - M_{\text{wd},i}$, where $M_{\text{wd},i}$ is the initial white dwarf mass, $M_{\text{wd}} = M_{\text{wd},i} (1 - 4k^2\omega/3)^{-3/4}$ is the final white dwarf mass, and k is the radius of gyration (Langer et al. 2000). With $k \approx 0.4$ and $\omega = 1 - (L_{\text{bl}}/L_{\text{disk}})^{1/2} \approx 0.78_{-0.26}^{+0.08}$, $\Delta M \approx 0.13 M_{\text{wd}} \sim 0.1 M_{\odot}$. If rapid rotation is the cause of SS Cyg's low boundary layer luminosity, the white dwarf angular velocity $\Omega_{\text{wd}} = \omega \Omega_{\text{K}}(R_{\text{wd}}) \approx 0.7_{-0.2}^{+0.1} \text{ Hz}$, hence the spin period $P_{\text{spin}} \approx 9_{-1}^{+4} \text{ s}$ (comparable to the period of the quasi-coherent oscillations), the rotation velocity $V_{\text{rot}} = \Omega_{\text{wd}} R_{\text{wd}} \approx 3800_{-1300}^{+400} \text{ km s}^{-1}$, and $V_{\text{rot}} \sin i \sim 2300 \text{ km s}^{-1}$. This last quantity is rather large, given that $V_{\text{rot}} \sin i \approx 1200 \text{ km s}^{-1}$ for WZ Sge and $V_{\text{rot}} \sin i \lesssim 400 \text{ km s}^{-1}$ for six other nonmagnetic CVs (Sion 1999).

Finally, we note that in the single scattering limit, conservation of momentum limits the mass-loss rate of a radiatively driven wind to $\dot{M}_{\text{max}} = L/V_{\infty} c$, where L is the system luminosity and V_{∞} is the wind terminal velocity. For SS Cyg in out-

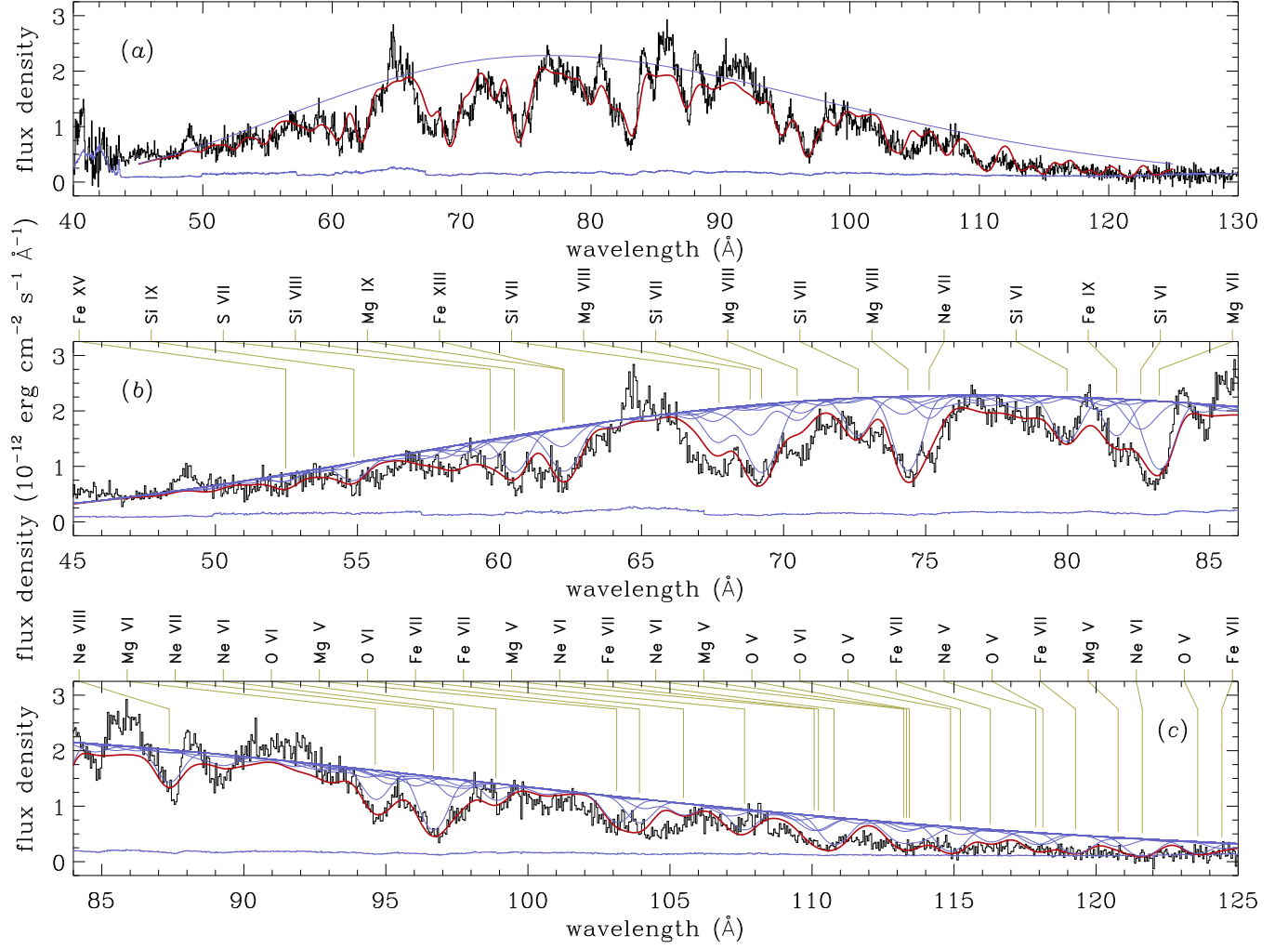


FIG. 3.— *Chandra* LETG/HRC spectrum and best-fit model spectrum of SS Cyg in outburst. Data are shown by the black histogram, the 1σ error vector by the blue histogram, the absorbed blackbody continuum by the smooth blue curve, and the net model spectrum by the thick red curve. In panels (b) and (c) the individual ion spectra are shown by the blue curves and the strongest lines in the model are labeled.

burst, $L = L_{\text{disk}} + L_{\text{bl}} \approx 1 \times 10^{35} \text{ erg s}^{-1}$ and $V_{\infty} \approx 3000 \text{ km s}^{-1}$, so $\dot{M}_{\text{max}} \approx 1 \times 10^{16} \text{ g s}^{-1}$. We derived a wind mass-loss rate $\dot{M}_{\text{w}} \approx 1 \times 10^{16} \text{ g s}^{-1}$ for SS Cyg in outburst, so $\dot{M}_{\text{w}}/\dot{M}_{\text{max}} \approx 1$. In τ Sco (B0 V), P Cyg (B1 Ia⁺), ζ Pup (O4 f), and ϵ Ori (B0 Ia) $\dot{M}_{\text{w}}/\dot{M}_{\text{max}} = 0.02, 0.22, 0.33$, and 0.65 , but in WR1 (WN5) $\dot{M}_{\text{w}}/\dot{M}_{\text{max}} = 60$ (Lamers & Cassinelli 1999), so we cannot conclude from this result that a mechanism other than radiation pressure is needed to drive the wind of SS Cyg.

5. SUMMARY

We have fitted the *Chandra* LETG spectrum of SS Cyg in outburst with a single temperature blackbody suffering the photoelectric opacity of a neutral column density and the scattering opacity of an outflowing wind. Figures 2 and 3 show that this simple model is capable of reproducing the essential features of the observed spectrum with $T_{\text{bl}} \approx 250 \pm 50 \text{ kK}$, $N_{\text{H}} \approx 5.0^{+2.9}_{-1.5} \times 10^{19} \text{ cm}^{-2}$, $f \approx 5.6^{+60}_{-4.5} \times 10^{-3}$, $L_{\text{bl}} \approx 5^{+18}_{-3} \times 10^{33} \text{ erg s}^{-1}$, and the wind velocity $v \approx 2500 \text{ km s}^{-1}$, mass-loss rate $\dot{M}_{\text{w}} \approx 1.1 \times 10^{16} \text{ g s}^{-1}$, and ionization fractions X listed in Table 1 ($X = 1$ otherwise). Given that in outburst the accretion disk luminosity $L_{\text{disk}} \approx 1 \times 10^{35} \text{ erg s}^{-1}$, $L_{\text{bl}}/L_{\text{disk}} \approx 0.05^{+0.18}_{-0.03}$, which can be explained if the white dwarf (or an equatorial belt thereon) is rotating with an angular velocity $\Omega_{\text{wd}} \approx 0.7^{+0.1}_{-0.2} \text{ Hz}$, hence $V_{\text{rot}} \sin i \sim 2300 \text{ km s}^{-1}$.

We have now used our simple one dimensional spectral model to fit the *EUVE* spectrum of OY Car in superoutburst (Mauche & Raymond 2000) and the *Chandra* LETG spectra of WZ Sge in superoutburst (Wheatley & Mauche 2004, in preparation) and SS Cyg in outburst. Although the model is unable to reproduce the asymmetries of the EUV emission features of OY Car and WZ Sge, or to produce an acceptable fit

to the EUV spectrum of SS Cyg even with arbitrary values of the ionization fractions, we believe that it captures the essential physics responsible for shaping the EUV spectra of these systems, and that it returns reasonable estimates of the values of the physical parameters that describe the boundary layer (effective temperature, emitting area, luminosity) and wind (velocity and mass-loss rate) of high- \dot{M} CVs. To make further progress in this area, we need to expand the model from one dimension to three dimensions; account for the velocity, density, and ionization structure of the wind; and compute the paths of boundary layer photons as they scatter in the wind. This could be accomplished with a Monte Carlo radiation transfer code, which we are in the process of developing (Mauche et al. 2004).

Our pre-approved *Chandra* target-of-opportunity observation of SS Cyg was made possible by the optical monitoring and alerts provided by the members, staff (particularly E. Waagen), and director, J. Mattei, of the AAVSO, and by the efforts of *Chandra* X-Ray Observatory Center Director H. Tananbaum, Mission Planner K. Delain, and the *Chandra* Flight Operations Team at MIT. We acknowledge with thanks the variable star observations from the AAVSO International Database contributed by observers worldwide and used in this research. Support for this work was provided by NASA through *Chandra* Award Number GO1-2023A issued by the *Chandra* X-Ray Observatory Center, which is operated by the Smithsonian Astrophysical Observatory for and on behalf of NASA under contract NAS8-39073. This work was performed under the auspices of the US Department of Energy by University of California, Lawrence Livermore National Laboratory under contract W-7405-Eng-48.

REFERENCES

- Anders, E., & Grevesse, N. 1989, *Geochim. Cosmochim. Acta*, 53, 197
Harrison, T. E., McNamara, B. J., Szkody, P., & Gilliland, R. L. 2000, *AJ*, 120, 2649
Lamers, H. J. G. L. M., & Cassinelli, J. P. 1999, *Introduction to Stellar Winds* (Cambridge: Cambridge Univ. Press)
Langer, N., Deutschmann, A., Wellstein, S., & Höflich, P. 2000, *A&A*, 362, 1046
Long, K. S., Mauche, C. W., Raymond, J. C., Szkody, P., & Mattei, J. A. 1996, *ApJ*, 469, 841
Mattei, J. A. 2003, Observations from the AAVSO International Database, personal communication
Mauche, C. W. 1996, in *Cataclysmic Variables and Related Objects*, ed. A. Evans & J. H. Wood (Dordrecht: Kluwer), 243
Mauche, C. W. 2002, *ApJ*, 580, 423
Mauche, C. W. 2004, in *X-Ray Timing 2003: Rossi and Beyond*, ed. P. Kaaret, F. K. Lamb, & J. H. Swank (Melville, NY: AIP), in press [astro-ph/0401484]
Mauche, C. W., Liedahl, D. A., Mathiese, B. F., Jimenez-Garate, M. A., & Raymond, J. C. 2004, *ApJ*, in press [astro-ph/0401328]
Mauche, C. W., Mattei, J. A., & Bateson, F. M. 2001, in *Evolution of Binary and Multiple Stars*, ed. Ph. Podsiadlowski, S. Rappaport, A. R. King, F. D'Antona, & L. Burderi (San Francisco: ASP), 367
Mauche, C. W., & Raymond, J. C. 2000, *ApJ*, 541, 924
Mauche, C. W., Raymond, J. C., & Córdova, F. A. 1988, *ApJ*, 335, 829
Mauche, C. W., Raymond, J. C., & Mattei, J. A. 1995, *ApJ*, 446, 842
Mukai, K., Wood, J. H., Naylor, T., Schlegel, E. M., & Swank, J. H. 1997, *ApJ*, 475, 812
Naylor, T., et al. 1988, *MNRAS*, 231, 237
Polidan, R. S., & Holberg, J. B. 1984, *Nature*, 309, 528
Popham, R., & Narayan, R. 1995, *ApJ*, 442, 337
Pratt, G. W., Hassall, B. J. M., Naylor, T., & Wood, J. H. 1999a, *MNRAS*, 307, 413
Pratt, G. W., Hassall, B. J. M., Naylor, T., Wood, J. H., & Patterson, J. 1999b, *MNRAS*, 309, 847
Pratt, G. W., Mukai, K., Hassall, B. J. M., Naylor, T., & Wood, J. H. 2004, *MNRAS*, 348, L49
Rumph, T., Bowyer, S., & Vennes, S. 1994, *AJ*, 107, 2108
Sion, E. M. 1999, *PASP*, 111, 532
Warner, B. 2004, *PASP*, 116, 115
Wheatley, P. J., Mauche, C. W., & Mattei, J. A. 2003, *MNRAS*, 345, 49
Wheatley, P. J., & West, R. G. 2003, *MNRAS*, 345, 1009
Wood, J. H., Naylor, T., Hassall, B. J. M., & Ramseyer, T. F. 1995, *MNRAS*, 273, 772
Wood, J. H., Naylor, T., & Marsh, T. R. 1995, *MNRAS*, 274, 31
van Teeseling, A. 1997, *A&A*, 319, L25
Verner, D. A., Verner, E. M., & Ferland, G. J. 1996, *Atomic Data and Nuc. Data Tables*, 64, 1